



SPECIAL ISSUE: Innovative Electrode Materials for Supercapacitors

Flexible all-solid-state micro-supercapacitor based on Ni fiber electrode coated with MnO₂ and reduced graphene oxide *via* electrochemical deposition

Jinhua Zhou^{1,2†}, Ningna Chen^{2†}, You Ge¹, Hongli Zhu¹, Xiaomiao Feng^{1*}, Ruiqing Liu¹, Yanwen Ma¹, Lianhui Wang¹ and Wenhua Hou^{2*}

ABSTRACT Flexible and micro-sized energy conversion/storage components are extremely demanding in portable and multifunctional electronic devices, especially those small, flexible, roll-up and even wearable ones. Here in this paper, a two-step electrochemical deposition method has been developed to coat Ni fibers with reduced graphene oxide and MnO₂ subsequently, giving rise to Ni@reduced-graphene-oxide@MnO₂ sheath-core flexible electrode with a high areal specific capacitance of 119.4 mF cm⁻² at a current density of 0.5 mA cm⁻² in 1 mol L⁻¹ Na₂SO₄ electrolyte. Using polyvinyl alcohol (PVA)-LiCl as a solid state electrolyte, two Ni@reduced-graphene-oxide@MnO₂ flexible electrodes were assembled into a free-standing, lightweight, symmetrical fiber-shaped micro-supercapacitor device with a maximum areal capacitance of 26.9 mF cm⁻². A high power density of 0.1 W cm⁻³ could be obtained when the energy density was as high as 0.27 mW h cm⁻³. Moreover, the resulting micro-supercapacitor device also demonstrated good flexibility and high cyclic stability. The present work provides a simple, facile and low-cost method for the fabrication of flexible, lightweight and wearable energy conversion/storage micro-devices with a high-performance.

Keywords: supercapacitor, flexible, fiber-shaped, MnO₂, graphene oxide, electrochemical deposition

INTRODUCTION

As one kind of important devices for energy storage, supercapacitors (SCs, also named electrochemical capacitors) can operate at a high charge/discharge rate over a

large number of cycles, bridging the gap between high energy batteries and high power conventional electrostatic capacitors [1,2]. Generally, SCs can be divided into two major categories according to the energy storage mechanism. The first category is electrochemical double layer capacitor (EDLC) which stores electrochemical energy through the physical charge accumulation at the electrode/electrolyte interface. The second category is pseudo-capacitor mainly based on the fast surface faradaic redox reactions. Relatively speaking, EDLC has a better rate capability, a higher power density, a longer operation life but a smaller capacitance and thus a lower energy density than pseudo-capacitor. This is dependent on their different electrical behaviors and ways of storing energy.

The performances of supercapacitors are generally determined by the electrode materials [3,4]. Up to now, various materials have been widely investigated as electrode materials for SCs, including carbon materials, conducting polymers [5] and metal oxides/hydroxides. Carbon materials, such as activated carbon [6], carbon nanotubes (CNTs) [7] and graphene [8,9], are normally used as electrode materials in EDLCs while conducting polymers and metal oxides/hydroxides in pseudo-capacitors. Among metal oxides/hydroxides (e.g., RuO₂, MnO₂, Co₃O₄, Ni(OH)₂) [10–14], MnO₂ is one of the most attractive materials because of its high theoretical pseudo-capacitance, low cost and environmental compatibility [4,15–17].

The recent rapid advance and eagerness of miniatur-

¹ Key Laboratory for Organic Electronics and Information Displays & Institute of Advanced Materials (IAM), Jiangsu National Synergistic Innovation Center for Advanced Materials (SICAM), Nanjing University of Posts & Telecommunications, Nanjing 210023, China

² Key Laboratory of Mesoscopic Chemistry, School of Chemistry and Chemical Engineering, Nanjing University, Nanjing 210023, China

[†] These authors contributed equally to this work.

* Corresponding authors (emails: iamxmfeng@njupt.edu.cn (Feng X); whou@nju.edu.cn (Hou W))

ized, portable consumer electronics have stimulated the development of power sources towards the trends of flexible/bendable electronic equipment such as wearable devices, foldable/roll-up displays, wireless sensors, smart chips and flexible mobile phones [18–20]. Various flexible energy storage devices have been developed to power the flexible/bendable electronic equipment, such as flexible supercapacitors [21–23], flexible Li-ion batteries [24] and flexible rechargeable batteries [25].

As one of the key energy storage devices, conventional supercapacitors are still too heavy, thick, rigid and bulky to fully meet the practical requirements for portable devices due to the presence of inactive components such as metal substrates, binders and conductive additives [26]. In order to meet the growing demands of modern society, some reformations were brought into SCs to make them small, thin, lightweight, flexible and even wearable.

Recently, flexible supercapacitors (FSCs) with diversified micro-structures and macro-features have been reported, in which each component (electrodes and packing shell, etc.) is flexible and thus FSCs are endowed with variable shapes. Considering that the key to fabricating FSCs generally lies in the acquirement of appropriate flexible electrodes (FEs), many researchers have devoted their efforts to the design of high performance FEs. According to their micro-structures and macroscopic patterns, the commonly reported FEs/FSCs are fiber-shaped, paper-like and three-dimensional (3D) porous FEs/FSCs, respectively [27–29]. Being different from paper-like and 3D porous FSCs, fiber-shaped FSCs are featured with a great flexibility and mechanical strength and thus exhibit unique and promising application prospect that they could be woven or knitted into fabrics/textiles to further produce wearable and smart clothes [30,31].

Graphene, a monolayer or few-layer honeycomb of carbon atoms, has been demonstrated to be a very promising candidate as electrode material for flexible supercapacitors. Competitive advantages of the graphene-based materials include large specific surface area, excellent electrical conductivity and high mechanical strength [20,32,33]. Via a dyeing approach, Zhao *et al.* [34] recently reported reduced graphene oxide (rGO)-coated polypyrrole FE, delivering a specific capacitance of 12.3 F g^{-1} at a scan rate of 5 mV s^{-1} . Using an electro-deposition method, He *et al.* [35] prepared graphene-loaded MnO_2 FSCs with a high areal capacitance of 1.42 F cm^{-2} at a scan rate of 2 mV s^{-1} . Through a spontaneous redox reaction, Zhang *et al.* [36] obtained an FE of graphene-wrapped copper wires, giving a specific volumetric capacitance of 7.3 F cm^{-3} at a current density of

0.5 mA cm^{-2} . Overall, the reported approaches for coating process are rather high-cost and time-consuming, usually including “dipping and drying”, hydrothermal and chemical reaction. Moreover, the electrochemical performances of FSCs still need to be improved.

Herein, we introduce an innovative design solution to achieve a high performance FSCs. By using Ni fiber as fibrous structural support, MnO_2 and rGO as active materials, Ni@rGO@ MnO_2 FEs could be obtained by a facile, time-saving and low-cost electrochemical deposition method. Furthermore, by using Ni@rGO@ MnO_2 FEs and polyvinyl alcohol (PVA)-LiCl as gel electrolyte, the symmetrical fiber-shaped FSCs were fabricated. The assembled FSC could deliver an areal specific capacitance of 26.9 mF cm^{-2} , a volumetric specific capacitance of 7.2 F cm^{-3} and a high power density of 0.1 W cm^{-3} when the energy density was as high as $0.27 \text{ mW h cm}^{-3}$ at a current density of 0.5 mA cm^{-2} . Moreover, the resulting FSC also demonstrated high cyclic stability and good flexibility.

EXPERIMENTAL SECTION

Chemicals

Natural graphite flake (about 325 mesh) and commercial Ni fibers (diameter about 0.15 mm) were purchased from Alfa Aesar Chemical Reagent Co. (USA). Manganese(II) acetate tetrahydrate ($\text{Mn}(\text{Ac})_2 \cdot 4\text{H}_2\text{O}$), sodium sulfate (Na_2SO_4), and lithium chloride (LiCl) were acquired from Sinopharm Chemical Reagent Co. (China). PVA was purchased from Aladdin Chemical Reagent Co. (USA). All reagents and solvents were of analytical grade and used as received without further treatment.

Preparation

Preparation of Ni@rGO@ MnO_2 electrode

GO was synthesized from graphite powder based on Hummer's method. The concentration of GO solution was about 3.5 mg mL^{-1} . A three-electrode system was used in the electrochemical deposition of rGO and MnO_2 on Ni fibers with a platinum wire as counter electrode and saturated calomel electrode (SCE) as reference electrode. The electrochemical deposition electrolyte contained 3.5 mg mL^{-1} GO solution, 1.0 mol L^{-1} Na_2SO_4 and 0.1 mol L^{-1} $\text{Mn}(\text{Ac})_2 \cdot 4\text{H}_2\text{O}$. Ni fiber was dipped into the electrolyte as working electrode and the electrochemical reduction of GO was performed at -1.0 V for 60 min and the deposition of MnO_2 at 1.0 V for 200 s. The mass load density of rGO on Ni fiber was about 0.025 mg cm^{-1} and

that of MnO_2 was about 0.05 mg cm^{-1} .

Preparation of fiber-shaped micro-supercapacitor

PVA-LiCl gel was prepared by adding 1.0 g of PVA and 1.0 g of LiCl into 10 mL of deionization (DI) water. The mixture was stirred until the solution became clear, and the resulting solution was used as both the ionic electrolyte and separator. Next, two Ni@rGO@MnO_2 FEs were immersed in the PVA-LiCl gel solution for 5 min, and then fixed on transparent poly(ethylene terephthalate) (PET) parallel to each other.

Electrochemical investigation

For single electrode tests, three electrodes were performed in $1.0 \text{ mol L}^{-1} \text{ Na}_2\text{SO}_4$ with a gauze platinum and an SCE as the counter and reference electrodes, respectively. The areal specific capacitance (C_A) could be calculated from the cyclic voltammograms (CV) curves according to Equation (1) [37]:

$$C_A = (\int IdV) / (S\Delta Vv), \quad (1)$$

where I is the response current, ΔV is the potential window, v is the scan rate, and S is the area of single electrode. The areal specific capacitance was calculated from the galvanostatic charge/discharge (GCD) curves using Equation (2) [38]:

$$C_A = I\Delta t / (S\Delta V), \quad (2)$$

where I represents the discharge current, Δt is the discharge time, S is the area of single electrode, and ΔV is the potential window. The volumetric capacitance (C_V) of the electrode was derived from the Equation (3) [36]:

$$C_V = C_A \times S / V, \quad (3)$$

where V is the volume of the fiber electrode.

Characterization

The morphologies of samples were characterized by scanning electron microscopy (SEM, S-4800) and transmission electron microscopy (TEM, JEOL-JEM-2100F at 100 kV, Japan). Fourier-transform infrared (FTIR) spectra of the products in KBr pellets were achieved on a Bruker model VECTOR22 Fourier transform spectrometer (Germany). The X-ray photoelectron spectroscopic (XPS) analysis was performed using an ESCALABMK II X-ray photoelectron spectrometer. Electrochemical experiments were carried out on a CHI660C electrochemical workstation (Chenhua, China). The three-electrode tests were performed in $1 \text{ mol L}^{-1} \text{ Na}_2\text{SO}_4$ with a platinum wire as counter electrode and SCE as reference electrode.

RESULTS AND DISCUSSION

As shown in Fig. 1, Ni fiber with a diameter about 0.15 mm played a role as working electrode in a three-electrode system with GO suspension and Mn^{2+} in electrolyte. When a negative voltage was applied to the Ni fiber, the GO was electrochemically reduced and stacked tightly in a parallel direction onto the surface of Ni fiber substrate. Then, the voltage was changed to positive, Mn^{2+} was oxidized and MnO_2 was generated on the surface of rGO/Ni fiber to obtain Ni@rGO@MnO_2 FEs. As a fibrous structural support for the deposition of MnO_2 and rGO, Ni metal fiber is flexible, mechanically robust and highly conductive. On the other hand, the rGO/ MnO_2 composite shell material can provide a high electrochemical capacitance. Two Ni@rGO@MnO_2 FEs were transferred in parallel onto flexible PET. These two electrodes were further fixed to the PET substrate by copper conductive adhesive. Finally, mixed PVA-LiCl gel electrolyte was coated on Ni@rGO@MnO_2 FEs, resulting in the formation of all-solid-state fiber-shaped FSCs in which the highly conductive Ni metal fiber played the role as current collector and PVA-LiCl gel electrolyte served as a separator to prevent short circuit inside FSC. Hence, no additional current collectors and separator were needed during the process.

The morphologies of the as-prepared Ni@rGO@MnO_2 FEs were characterized through SEM images. Fig. 2a shows a top-view SEM image of Ni fiber after deposition of rGO, and it can be observed that Ni fiber is wrapped with rGO nanosheets tightly and uniformly. In addition, the characteristics of wrinkle and gully of graphene are clearly visible from Fig. 2b. As shown in Fig. 2c, after deposition of MnO_2 , the entire graphene networks are uniformly covered with a layer of MnO_2 nanomaterials and the resulting Ni@rGO@MnO_2 FE has an increased diameter about $160 \mu\text{m}$. A higher magnification image shows that the coated MnO_2 has an alveolate microstructure composed of nanosheets (Fig. 2d). Fig. S1c (see Supplementary information) shows a cross-sectional SEM image of Ni@rGO@MnO_2 fibers. The shell thickness of MnO_2 /rGO coated on Ni fiber is around $10 \mu\text{m}$. And rGO layers are stacked in parallel direction, forming a layer-by-layer structure (Fig. S1d). The coated rGO and MnO_2 /rGO were peeled from Ni fibers *via* simple ultrasonic process, and their morphologies and microstructures were further investigated by TEM images. As shown in Fig. 2e, the resulting rGO nanosheets are typical transparent and curly with folded wrinkles. On the other hand, MnO_2 /rGO shows a morphology of the interconnected MnO_2 nanosheets on the surface of rGO (Fig. 2f), being

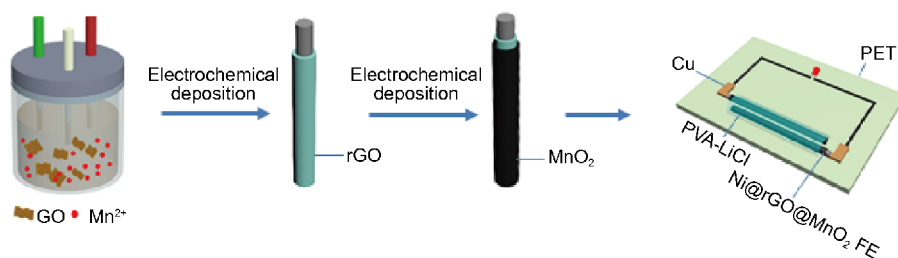


Figure 1 Schematic illustration for the fabrication process of Ni@rGO@MnO₂ FE *via* electrochemical deposition and the symmetrical FSC composed of two Ni@rGO@MnO₂ FEs.

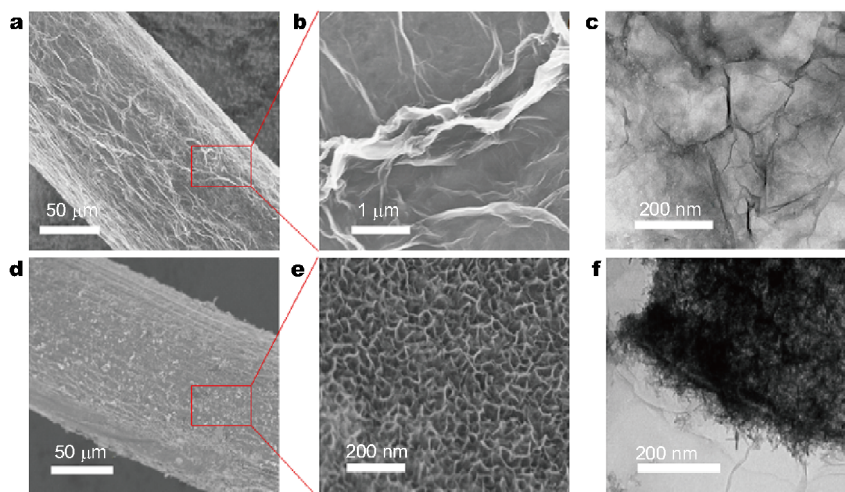


Figure 2 SEM images of Ni@rGO FE (a, b), Ni@rGO@MnO₂ FE (c, d), TEM images of rGO peeled from Ni@rGO FE (e) and MnO₂/rGO peeled from Ni@rGO@MnO₂ FE (f).

consistent with the SEM results.

Fig. 3a shows FTIR spectra of GO, rGO and MnO₂/rGO. The spectrum of GO reveals strong absorption peaks at 1734, 1623, 1402, and 1104 cm⁻¹, which correspond to the C=O stretching vibration from carbonyl and carboxylic groups, skeletal vibration of aromatic C=C, carboxy -COOH group and alkoxy C-O group, respectively [19]. By comparison, the intensities of these absorption peaks are dramatically decreased in rGO, suggesting that most of oxygen-containing groups have been removed *via* electrochemical reduction. For MnO₂/rGO, a strong and wide absorption peaks appears around 525 cm⁻¹, corresponding to the Mn-O vibrations of MnO₂ [12]. Fig. 3b shows the XRD pattern of MnO₂/rGO, in which most of the diffraction peaks can be well indexed to MnO₂ (PDF# 53-0633). In addition, the broad peak between 22° and 27° is in agreement with the (002) reflection of the stacked rGO sheets.

XPS spectra were recorded to further reveal the surface

chemical compositions. As shown in Fig. 4a, besides those of C and O, the signal of Mn also appears in the survey spectrum of MnO₂/rGO, indicating the attachment of MnO₂ on the surface of rGO. Fig. 4b shows the C 1s XPS spectra of GO and MnO₂/rGO, and both can be deconvoluted into four peaks of C-C/C=C (284.6 eV), C-O (286.4 eV), C=O (287.0 eV), and O=C-OH (288.5 eV) [39]. By comparison, the peak intensity of oxygen-containing functional groups in rGO is decreased significantly, indicating that GO was reduced to rGO after electrochemical reduction. As shown in Fig. 4c, the Mn 2p XPS spectrum shows Mn 2p_{3/2} peak located at 641.6 eV and Mn 2p_{1/2} peak at 653.2 eV, with a spin-energy separation of 11.6 eV, indicating that the Mn element mainly exists as Mn⁴⁺ in the sample [40].

The electrochemical characteristics of the as-prepared Ni@rGO@MnO₂ FEs were investigated in a three-electrode system in 1.0 mol L⁻¹ aqueous Na₂SO₄ electrolyte. We decorated rGO on Ni fiber by varying the deposition

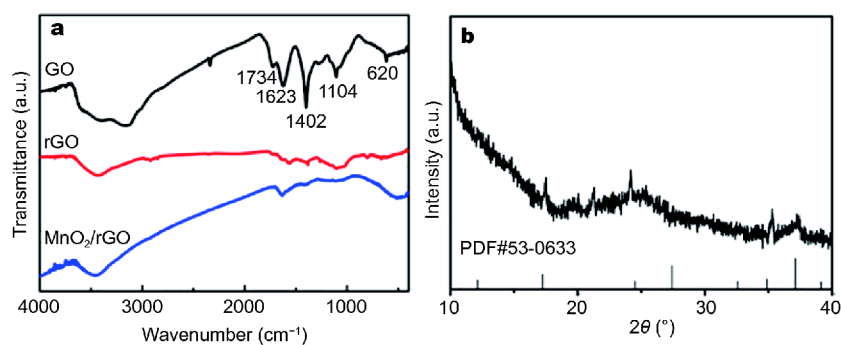


Figure 3 (a) FTIR spectra of GO, rGO and MnO₂/rGO; (b) XRD pattern of MnO₂/rGO.

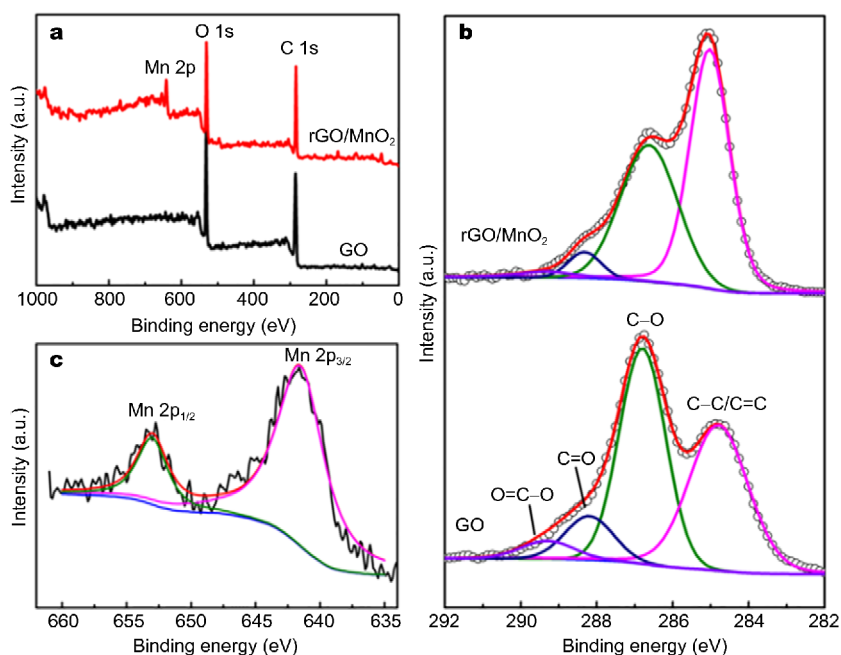


Figure 4 XPS spectra survey scan of GO and MnO₂/rGO (a), C 1s of GO and MnO₂/rGO (b), Mn 2p of MnO₂/rGO (c).

time and it was found that the current was increased with the deposition time in the corresponding CV curves (Fig. S2). When the deposition time exceeded 60 min, the deposited rGO on Ni fiber could be easily exfoliated because of too much rGO loaded. Therefore, in the subsequent deposition of MnO₂, we adopted an rGO deposition time of 60 min and its electrochemical characteristics were measured first. As shown in Fig. S3, the CV curves show an ideal rectangular shape and the corresponding GCD curves are almost symmetrical, indicating the ideal EDLC behavior of rGO@Ni FE. After that, MnO₂ was decorated on rGO@Ni FE by changing the deposition time. It was found that as the deposition time was increased, the CV current of Ni@rGO@MnO₂ FE was increased and the most

obvious increase was observed for the sample with a deposition time of 200 s (Fig. S4). We compared the electrochemical performances of Ni@rGO, Ni@MnO₂ and Ni@rGO@MnO₂ FEs in 1 mol L⁻¹ Na₂SO₄ (Fig. S5). Both CV and GCD measurements revealed the Ni@rGO@MnO₂ FEs had been equipped with most excellent electrochemical performance. The areal capacitance of Ni@rGO@MnO₂ FE is 2.3 times that of the pristine Ni@MnO₂ FE and 10 times that of Ni@rGO FE at the same current density, giving a clear evidence of the synergistic effect between MnO₂ and rGO in the composite. Hence, in the following experiments, the electrochemical performances of Ni@rGO@MnO₂ FE obtained with an rGO deposition time of 60 min and a MnO₂ deposition

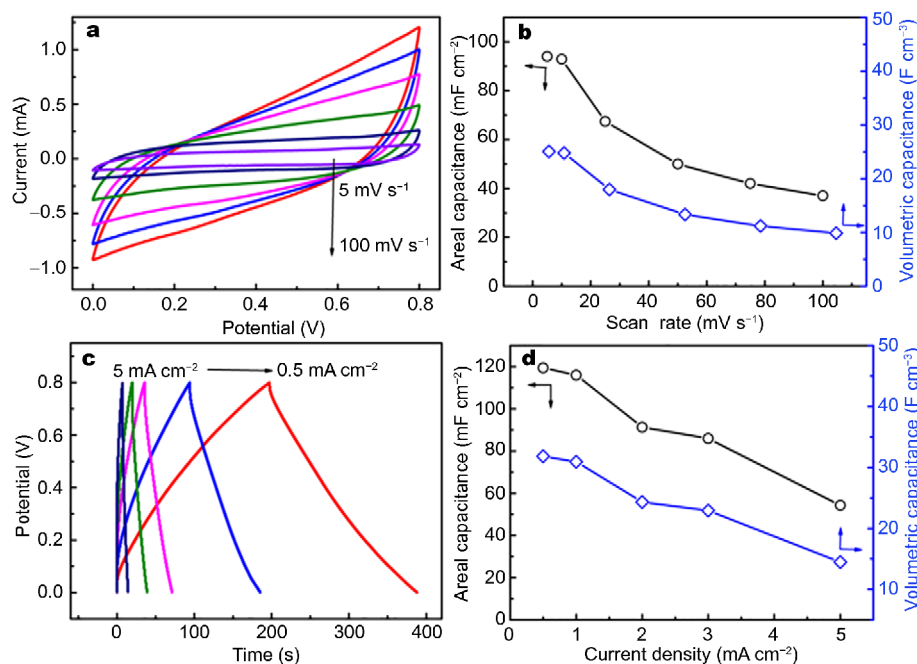


Figure 5 CV curves (a) and corresponding specific capacitances (b) of Ni@rGO@MnO₂ FE at different scan rates in 1 mol L⁻¹ Na₂SO₄; GCD curves (c) and corresponding specific capacitances (d) of Ni@rGO@MnO₂ FE at different current densities in 1 mol L⁻¹ Na₂SO₄.

time of 200 s were systematically studied.

Fig. 5a shows CV curves of Ni@rGO@MnO₂ FE at different scan rates in 1 mol L⁻¹ Na₂SO₄. A deviation from rectangular shape can be observed due to the pseudo-capacitive contribution from MnO₂ along with the double layer contribution from graphene. When the scan rate is increased from 5 to 100 mV s⁻¹, the calculated areal specific capacitance (C_A) values are 94.0, 92.9, 67.4, 50.0, 42.0 and 37.0 mF cm⁻² and the corresponding volumetric specific capacitance (C_V) are 25.1, 24.8, 18.0, 13.3, 11.2 and 9.9 F cm⁻³, respectively. On the other hand, the GCD curves show a linear and nearly symmetrical shape, indicating the typical characteristic of an ideal supercapacitor. The calculated C_A are 119.4, 116, 91.3, 86.0 and 54.3 mF cm⁻² and C_V are 31.8, 30.9, 24.3, 22.9 and 14.5 F cm⁻³ at a series of current densities of 0.5, 1.0, 2.0, 3.0 and 5.0 mA cm⁻², respectively. The energy storage in Ni@rGO@MnO₂ FE is realized through both the electrostatic accumulation of charges on rGO and the reversible redox reactions on MnO₂. The electrochemical impedances of Ni@rGO, Ni@MnO₂ and Ni@rGO@MnO₂ FEs were measured at a frequency range of 0.01 Hz to 100 kHz. As shown in Fig. S6, all plots display a part of semicircle at high-frequency region and a straight line in the low-frequency region, corresponding to the electron-transfer process and diffusion process, respectively [41].

At the low-frequency region, both Ni@rGO and Ni@rGO@MnO₂ FEs show a more vertical line than Ni@MnO₂ FE, indicating a better capacitive behavior and a lower ion diffusion resistance. At the high-frequency region, Ni@MnO₂ FE obviously has the highest charge transfer resistance (R_{ct} , a semicircle in the high-frequency region), while both Ni@rGO and Ni@rGO@MnO₂ FEs show greatly decreased R_{ct} due to the good electronic conductivity of rGO. The inset is the corresponding equivalent circuit, where R_s is the solution resistance, R_{ct} is the interfacial charge transfer resistance and W_s is the Warburg impedance. The calculated values of equivalent series resistance (ESR, $R_s + R_{ct}$) are 28, 50 and 400 Ω for Ni@rGO, Ni@rGO@MnO₂ and Ni@MnO₂ FEs, respectively [42,43]. The cycle stability of Ni@rGO@MnO₂ FE was measured at a current density of 1 mA cm⁻² in 1 mol L⁻¹ Na₂SO₄. Fig. S7 shows 90% retention after 5,000 charge-discharge cycles, indicating a quite remarkable cycle stability.

Two Ni@rGO@MnO₂ FEs were assembled into symmetrical fiber-shaped FSC by using PVA-LiCl gel as the solid electrolyte. Fig. 6a shows CV curves of the resulted FSC at different scan rates ranging from 5 to 200 mV s⁻¹. The CV curves display nearly mirror-like images and the relatively rectangular-like shapes, demonstrating an ideal capacitive behavior and a good reversibility. The calcu-

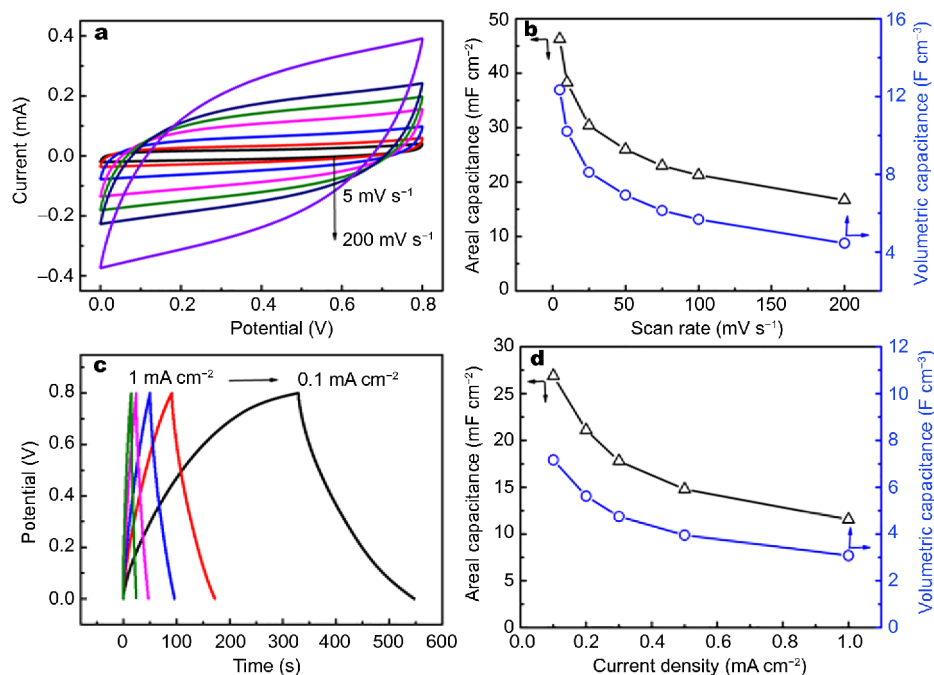


Figure 6 CV curves (a) and corresponding specific capacitances (b) of symmetrical fiber-shaped Ni@rGO@MnO₂ FSC at different scan rates; GCD curves (c) and corresponding specific capacitances (d) of symmetrical fiber-shaped Ni@rGO@MnO₂ FSC at different current densities.

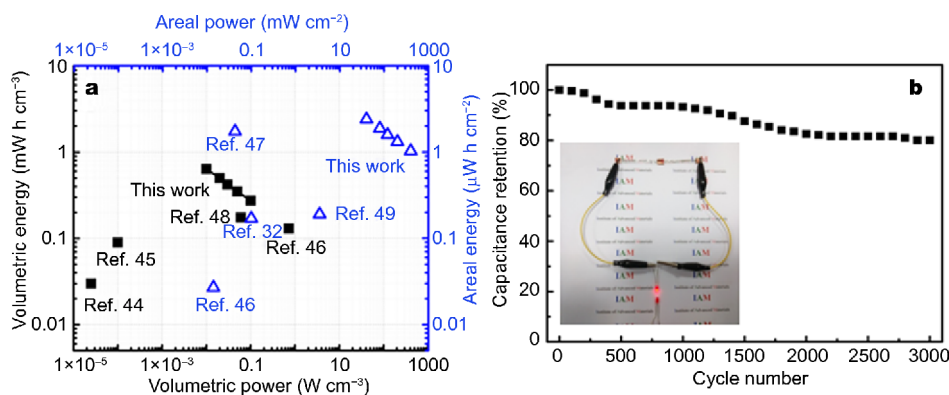


Figure 7 (a) Ragone plots of symmetrical fiber-shaped Ni@rGO@MnO₂ FSC and the comparison with the previous FSCs; (b) capacitance retention after 3000 charge-discharge cycles at a current density of 1 mA cm⁻² (inset: optical photo shows that two devices in series light a LED).

lated C_A are 46.3, 38.3, 30.4, 26.0, 23.0, 21.3, 16.7 mF cm⁻² at the scan rates of 5, 10, 25, 50, 75, 100, 200 mV s⁻¹ and the corresponding C_V are 12.3, 10.2, 8.1, 6.9, 6.1, 5.7 and 4.5 F cm⁻³, respectively. Fig. 6c shows the GCD curves of the resulting FSC at different current densities from 1 to 0.1 mA cm⁻². The nearly triangular shape confirms the formation of efficient electric double layers and the good charge propagation across the electrode. The calculated C_A from GCD curves are 26.9, 21.1, 17.8, 14.8 and 11.5 mF cm⁻² at the current densities of 0.1, 0.2, 0.3, 0.5 and

1.0 mA cm⁻² and the corresponding C_V are 7.2, 5.6, 4.7, 3.9 and 3.1 F cm⁻³, respectively.

To evaluate the energy storage performance of the resulting FSC, the energy density *versus* power density, i.e., Ragone chart, was plotted and shown in Fig. 7a. The volumetric energy density is varied from 0.64 to 0.27 mW h cm⁻³, and the areal energy density is ranged from 2.38 to 1.02 μW h cm⁻². Moreover, a high power density of 0.1 W cm⁻³ can be obtained when the energy density is as high as 0.27 mW h cm⁻³. These values are

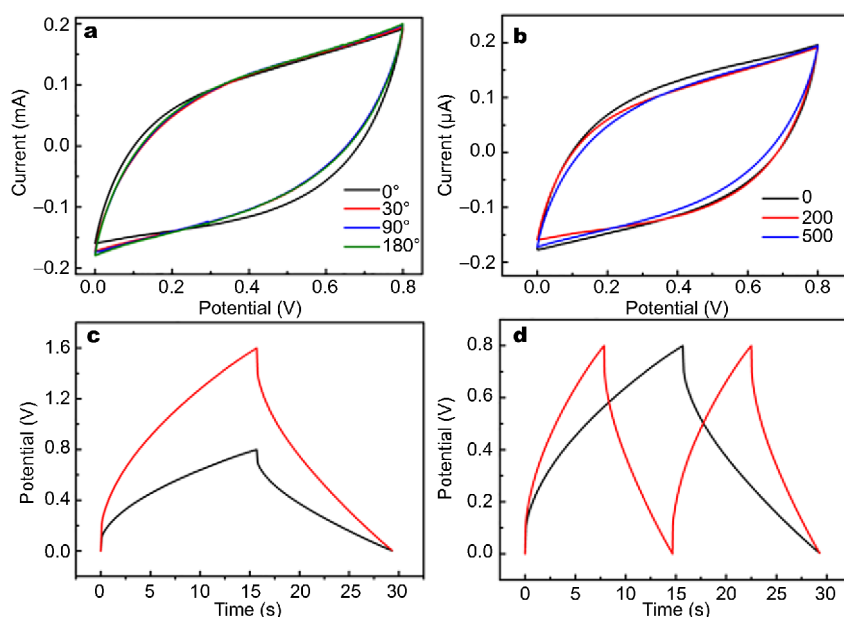


Figure 8 The CV curves of the symmetric fiber-shaped Ni@rGO@MnO₂ FSC device at 100 mV s⁻¹ with different bending angles (a) and bending cycle numbers (b). GCD curves of a single FSC (black lines) and two FSCs connected in series (c) and in parallel (d).

superior to the previously reports based on other materials such as SWCNTs (0.03 mW h cm⁻³ at 0.025 mW cm⁻³) [44], graphene (0.09 mW h cm⁻³ at 0.1 mW cm⁻³) [45], CNTs (0.13 mW h cm⁻³ at 0.73 W cm⁻³, 0.027 μW h cm⁻² at 0.014 mW cm⁻²) [46], all-graphene core-sheath fibers (0.17 μW h cm⁻² at 0.1 mW cm⁻²) [32], CNTs/ordered mesoporous carbon composite fibers (1.77 μW h cm⁻² at 0.043 mW cm⁻²) [47], MnO₂/carbon nanoparticles (0.06 mW h cm⁻³ at 0.175 mW cm⁻³) [48], and PEDOT/carbon fibers (3.5 μW h cm⁻² at 0.19 mW cm⁻²) [49]. The cycle stability is a vital factor for high-performance supercapacitors. Fig. 7b shows the corresponding GCD tests at a current density of 1 mA cm⁻². It can be seen that after 3000 cycles, 80% of the initial capacitance is retained, showing a good cyclic stability. The rGO layer can help electrode withstand the strain relaxation and mechanical deformation, preventing MnO₂ layer from seriously swelling/shrinking and polymer gel from over-oxidizing during the long charge/discharge process [50]. As shown in the inset of Fig. 7b, a red LED indicator can be driven by two fiber-shaped Ni@rGO@MnO₂ FSC devices in series, indicating their potential application in energy storage.

The performance of the resulting symmetrical fiber-shaped Ni@rGO@MnO₂ FSC under different bending angles and cycles was measured since the folding endurance is a very important parameter of flexible devices to show the mechanical strength. Fig. 8a, b display CV

curves of the flexible device at different bending angles and cycles. The corresponding digital photos of different bending angles were provided in Fig. S8. No obvious difference can be observed, indicating a highly flexibility and a good mechanical strength of the resulting symmetrical fiber-shaped Ni@rGO@MnO₂ FSC device. In order to meet the practical application of micro-supercapacitors, it is necessary to connect the supercapacitors in series and/or in parallel to increase the operating voltage and/or the current in some situations. Fig. 8c, d show the charge/discharge curves of two devices in series and in parallel at a current density of 0.5 mA cm⁻², respectively. The GCD curves exhibit ideal symmetric and triangular shapes, which is consistent with the individual device. Meanwhile, the operating voltage window and capacitance are doubled under the same test conditions, revealing that the micro-supercapacitor well obeys the basic rule of series and parallel connections.

CONCLUSION

We have successfully developed a two-step electrochemical deposition method to coat rGO and MnO₂ on Ni fiber. Here, MnO₂/rGO played the role of electrochemically active electrode materials while Ni fiber served as a flexible structural support. The resulting fiber-shaped Ni@rGO@MnO₂ FE showed an areal specific capacitance of 119.4 mF cm⁻² and a volumetric specific capacitance of 31.8 F cm⁻³ at a current density of 0.5 mA cm⁻² in

1 mol L⁻¹ Na₂SO₄, due to the synergistic effect between rGO and MnO₂. Two Ni@rGO/MnO₂ FEs were assembled into a symmetrical, flexible and fiber-shaped micro-supercapacitor by using PVA-LiCl gel as the solid electrolyte, and the obtained micro-supercapacitor exhibited an areal specific capacitance of 26.9 mF cm⁻² and a volumetric specific capacitance of 7.2 F cm⁻³ at 0.1 mA cm⁻². Moreover, a high power density of 0.1 W cm⁻³ could be obtained when the energy density was as high as 0.27 mW h cm⁻³. The obtained FSC not only possessed an excellent electrochemical performance but also a high flexibility and a good mechanical strength, being robust enough to sustain deformations under different bending angles and cycles. To extend the practical applications of micro-supercapacitor, two micro-supercapacitor devices were further connected in series and in parallel, showing the doubled operating voltage window and capacitance. This research might provide a method for flexible, lightweight, high-performance, low-cost and environmentally friendly materials used in stretchable/bendable electronic devices, portable energy storage devices and flexible powering sustainable vehicles.

Received 5 September 2017; accepted 23 November 2017;
published online 19 January 2018

- Cheng JP, Zhang J, Liu F. Recent development of metal hydroxides as electrode material of electrochemical capacitors. *RSC Adv*, 2014, 4: 38893–38917
- Liu S, Sun S, You XZ. Inorganic nanostructured materials for high performance electrochemical supercapacitors. *Nanoscale*, 2014, 6: 2037–2045
- Wang G, Zhang L, Zhang J. A review of electrode materials for electrochemical supercapacitors. *Chem Soc Rev*, 2012, 41: 797–828
- Yu L, Zhang G, Yuan C, *et al.* Hierarchical NiCo₂O₄@MnO₂ core-shell heterostructured nanowire arrays on Ni foam as high-performance supercapacitor electrodes. *Chem Commun*, 2013, 49: 137–139
- Wang K, Zhang X, Sun X, *et al.* Conducting polymer hydrogel materials for high-performance flexible solid-state supercapacitors. *Sci China Mater*, 2016, 59: 412–420
- Frackowiak E, Béguin F. Carbon materials for the electrochemical storage of energy in capacitors. *Carbon*, 2001, 39: 937–950
- Futaba DN, Hata K, Yamada T, *et al.* Shape-engineerable and highly densely packed single-walled carbon nanotubes and their application as super-capacitor electrodes. *Nat Mater*, 2006, 5: 987–994
- Stoller MD, Park S, Zhu Y, *et al.* Graphene-based ultracapacitors. *Nano Lett*, 2008, 8: 3498–3502
- Wang DW, Li F, Zhao J, *et al.* Fabrication of graphene/polyaniline composite paper via *in situ* anodic electropolymerization for high-performance flexible electrode. *ACS Nano*, 2009, 3: 1745–1752
- Hu CC, Chang KH, Lin MC, *et al.* Design and tailoring of the nanotubular arrayed architecture of hydrous RuO₂ for next generation supercapacitors. *Nano Lett*, 2006, 6: 2690–2695
- Wang H, Casalongue HS, Liang Y, *et al.* Ni(OH)₂ nanoplates grown on graphene as advanced electrochemical pseudocapacitor materials. *J Am Chem Soc*, 2010, 132: 7472–7477
- Feng X, Yan Z, Chen N, *et al.* The synthesis of shape-controlled MnO₂/graphene composites via a facile one-step hydrothermal method and their application in supercapacitors. *J Mater Chem A*, 2013, 1: 12818–12825
- Wang H, Deng J, Chen Y, *et al.* Hydrothermal synthesis of manganese oxide encapsulated multiporous carbon nanofibers for supercapacitors. *Nano Res*, 2016, 9: 2672–2680
- Rakhi RB, Chen W, Hedhili MN, *et al.* Enhanced rate performance of mesoporous Co₃O₄ nanosheet supercapacitor electrodes by hydrous RuO₂ nanoparticle decoration. *ACS Appl Mater Interfaces*, 2014, 6: 4196–4206
- Wang H, Xu Z, Li Z, *et al.* Hybrid device employing three-dimensional arrays of MnO in carbon nanosheets bridges battery-supercapacitor divide. *Nano Lett*, 2014, 14: 1987–1994
- Chang HW, Lu YR, Chen JL, *et al.* Nanoflaky MnO₂/functionalized carbon nanotubes for supercapacitors: an *in situ* X-ray absorption spectroscopic investigation. *Nanoscale*, 2015, 7: 1725–1735
- Zhang Z, Chi K, Xiao F, *et al.* Advanced solid-state asymmetric supercapacitors based on 3D graphene/MnO₂ and graphene/poly-pyrrole hybrid architectures. *J Mater Chem A*, 2015, 3: 12828–12835
- Zhong J, Zhang Y, Zhong Q, *et al.* Fiber-based generator for wearable electronics and mobile medication. *ACS Nano*, 2014, 8: 6273–6280
- Xie B, Yang C, Zhang Z, *et al.* Shape-tailorable graphene-based ultra-high-rate supercapacitor for wearable electronics. *ACS Nano*, 2015, 9: 5636–5645
- Huang Y, Hu H, Huang Y, *et al.* From industrially weavable and knittable highly conductive yarns to large wearable energy storage textiles. *ACS Nano*, 2015, 9: 4766–4775
- Zhang X, Zhang H, Lin Z, *et al.* Recent advances and challenges of stretchable supercapacitors based on carbon materials. *Sci China Mater*, 2016, 59: 475–494
- Yu M, Cheng X, Zeng Y, *et al.* Dual-doped molybdenum trioxide nanowires: a bifunctional anode for fiber-shaped asymmetric supercapacitors and microbial fuel cells. *Angew Chem Int Ed*, 2016, 55: 6762–6766
- Yu M, Zhao S, Feng H, *et al.* Engineering thin MoS₂ nanosheets on TiN nanorods: advanced electrochemical capacitor electrode and hydrogen evolution electrocatalyst. *ACS Energy Lett*, 2017, 2: 1862–1868
- Dong X, Chen L, Su X, *et al.* Flexible aqueous lithium-ion battery with high safety and large volumetric energy density. *Angew Chem Int Ed*, 2016, 55: 7474–7477
- Zeng Y, Zhang X, Meng Y, *et al.* Achieving ultrahigh energy density and long durability in a flexible rechargeable quasi-solid-state Zn-MnO₂ battery. *Adv Mater*, 2017, 29: 1700274–1700281
- Wang Z, Carlsson DO, Tammela P, *et al.* Surface modified nanocellulose fibers yield conducting polymer-based flexible supercapacitors with enhanced capacitances. *ACS Nano*, 2015, 9: 7563–7571
- Dong L, Xu C, Yang Q, *et al.* High-performance compressible supercapacitors based on functionally synergic multiscale carbon composite textiles. *J Mater Chem A*, 2015, 3: 4729–4737
- Wang X, Liu B, Liu R, *et al.* Fiber-based flexible all-solid-state asymmetric supercapacitors for integrated photodetecting system. *Angew Chem Int Ed*, 2014, 53: 1849–1853

- 29 Wang Q, Wang X, Xu J, *et al.* Flexible coaxial-type fiber supercapacitor based on NiCo₂O₄ nanosheets electrodes. *Nano Energy*, 2014, 8: 44–51
- 30 Yu D, Qian Q, Wei L, *et al.* Emergence of fiber supercapacitors. *Chem Soc Rev*, 2015, 44: 647–662
- 31 Xu H, Hu X, Sun Y, *et al.* Flexible fiber-shaped supercapacitors based on hierarchically nanostructured composite electrodes. *Nano Res*, 2014, 8: 1148–1158
- 32 Meng Y, Zhao Y, Hu C, *et al.* All-graphene core-sheath microfibers for all-solid-state, stretchable fibriform supercapacitors and wearable electronic textiles. *Adv Mater*, 2013, 25: 2326–2331
- 33 Shao Y, El-Kady MF, Wang LJ, *et al.* Graphene-based materials for flexible supercapacitors. *Chem Soc Rev*, 2015, 44: 3639–3665
- 34 Zhao C, Shu K, Wang C, *et al.* Reduced graphene oxide and polypyrrole/reduced graphene oxide composite coated stretchable fabric electrodes for supercapacitor application. *Electrochim Acta*, 2015, 172: 12–19
- 35 He Y, Chen W, Li X, *et al.* Freestanding three-dimensional graphene/MnO₂ composite networks as ultralight and flexible supercapacitor electrodes. *ACS Nano*, 2013, 7: 174–182
- 36 Zhang Z, Xiao F, Wang S. Hierarchically structured MnO₂/graphene/carbon fiber and porous graphene hydrogel wrapped copper wire for fiber-based flexible all-solid-state asymmetric supercapacitors. *J Mater Chem A*, 2015, 3: 11215–11223
- 37 Zhu J, He J. Facile synthesis of graphene-wrapped honeycomb MnO₂ nanospheres and their application in supercapacitors. *ACS Appl Mater Interfaces*, 2012, 4: 1770–1776
- 38 Lai L, Yang H, Wang L, *et al.* Preparation of supercapacitor electrodes through selection of graphene surface functionalities. *ACS Nano*, 2012, 6: 5941–5951
- 39 Feng X, Zhou J, Wang L, *et al.* Synthesis of shape-controlled NiO-graphene nanocomposites with enhanced supercapacitive properties. *New J Chem*, 2015, 39: 4026–4034
- 40 Lai F, Miao YE, Huang Y, *et al.* Flexible hybrid membranes of NiCo₂O₄-doped carbon nanofiber@MnO₂ core-sheath nanostructures for high-performance supercapacitors. *J Phys Chem C*, 2015, 119: 13442–13450
- 41 Xie Y, Xia C, Du H, *et al.* Enhanced electrochemical performance of polyaniline/carbon/titanium nitride nanowire array for flexible supercapacitor. *J Power Sources*, 2015, 286: 561–570
- 42 Buller S, Karden E, Kok D, *et al.* Modeling the dynamic behavior of supercapacitors using impedance spectroscopy. In: Thirty-Sixth IAS Annual Meeting. Conference Record of the 2001 IEEE, 2001, 4: 2500–2504
- 43 Barcellona S, Piegari L. A lithium-ion capacitor model working on a wide temperature range. *J Power Sources*, 2017, 342: 241–251
- 44 Kaempgen M, Chan CK, Ma J, *et al.* Printable thin film supercapacitors using single-walled carbon nanotubes. *Nano Lett*, 2009, 9: 1872–1876
- 45 Kang YJ, Chung H, Han CH, *et al.* All-solid-state flexible supercapacitors based on papers coated with carbon nanotubes and ionic-liquid-based gel electrolytes. *Nanotechnology*, 2012, 23: 065401
- 46 Bae J, Song MK, Park YJ, *et al.* Fiber supercapacitors made of nanowire-fiber hybrid structures for wearable/flexible energy storage. *Angew Chem Int Ed*, 2011, 50: 1683–1687
- 47 Ren J, Bai W, Guan G, *et al.* Flexible and weavable capacitor wire based on a carbon nanocomposite fiber. *Adv Mater*, 2013, 25: 5965–5970
- 48 Yuan L, Lu XH, Xiao X, *et al.* Flexible solid-state supercapacitors based on carbon nanoparticles/MnO₂ nanorods hybrid structure. *ACS Nano*, 2011, 6: 656–661
- 49 Pandey GP, Rastogi AC, Westgate CR. All-solid-state supercapacitors with poly(3,4-ethylenedioxythiophene)-coated carbon fiber paper electrodes and ionic liquid gel polymer electrolyte. *J Power Sources*, 2014, 245: 857–865
- 50 Yu P, Li Y, Zhao X, *et al.* Graphene-wrapped polyaniline nanowire arrays on nitrogen-doped carbon fabric as novel flexible hybrid electrode materials for high-performance supercapacitor. *Langmuir*, 2014, 30: 5306–5313

Acknowledgements This work was supported by the Ministry of Education of China (IRT1148), the National Natural Science Foundation of China (51772157 and 21173116), Synergistic Innovation Center for Organic Electronics and Information Displays, Jiangsu Province “Six Talent Peak” (2015-JY-015), Jiangsu Provincial Natural Science Foundation (BK20141424), the Program of Nanjing University of Posts and Telecommunications (NY214088), and the Open Research Fund of State Key Laboratory of Bioelectronics of Southeast University (I2015010).

Author contributions Feng X and Ma Y designed and engineered this work; Zhou J, Chen N, Ge Y, Zhu H carried out the experiments. Zhou J and Hou W wrote this paper. All authors contributed to the general discussion.

Conflict of interest The authors declare no conflict of interest.

Supplementary information Supporting data are available in the online version of this paper.



Jinhua Zhou received her MSc degree under the supervision of Prof. Xiaomiao Feng in the Department of Materials Chemistry at the Nanjing University of Posts and Telecommunications in 2016. She is currently a PhD under the supervision of Prof. Wenhua Hou at Nanjing University. Her research is mainly focused on the synthesis of 2D materials, and their application for energy conversion and storage devices.



Ningna Chen obtained her MSc degree from Nanjing University of Posts & Telecommunications in 2015. Currently, she is pursuing her PhD degree under the supervision of Prof. Wenhua Hou at Nanjing University. Her research is mainly focused on the synthesis of two-dimensional layered transition metal oxide nanomaterials, and their application for energy conversion and storage devices.



Xiaomiao Feng is a Professor in the Department of Materials Chemistry at the Nanjing University of Posts and Telecommunications. She received her PhD from Nanjing University, Nanjing (China) in 2007. Between July 2012 and July 2013 she joined the research group of Prof. J. Wang at the Department of Nanoengineering, University of California, San Diego as a visiting scholar. Her research interests include nanomaterials, nanomachines, biosensors and super capacitors.



Wenhua Hou is a professor in the School of Chemistry and Chemical Engineering at Nanjing University. He received his BS (1985) and PhD (1993) in chemistry from Nanjing University. He worked as visiting scholar at the State University of New York at Albany and University of California, San Diego. His research interests include the synthesis of 2D layer nanomaterials for photocatalysis and energy storage.

电沉积制备氧化石墨烯/二氧化锰包裹镍纤维电极用于柔性固态超级电容器

周锦华^{1,2†}, 陈宁娜^{2†}, 葛优¹, 朱红丽¹, 冯晓苗^{1*}, 刘瑞卿¹, 马延文¹, 汪联辉¹, 侯文华^{2*}

摘要 便携式及多功能电子设备的不断进步要求为其提供动力能量的存储与转换器件向尺寸小、柔性、能够卷曲甚至可穿戴方向发展. 本文采用两步电化学沉积法依次将还原氧化石墨烯(rGO)和MnO₂沉积到镍纤维上得到Ni@rGO@MnO₂壳核结构的柔性电极. 该电极在1 mol L⁻¹ Na₂SO₄ 电解液中电流密度为0.5 mA cm⁻²时面积比电容为119.4 mF cm⁻². 以PVA-LiCl为固态电解液, 将两根Ni@rGO@MnO₂电极组装成自支撑、质轻、对称的纤维状微型超级电容器, 最大面积比电容为26.9 mF cm⁻², 能量密度高达0.1 W cm⁻³ (0.27 mW h cm⁻³). 此外, 该微型超级电容器还展现了良好的柔性和循环性能. 这项研究工作主要提供了一种简单、易操作、低成本的制备柔性、质轻、可穿戴的高性能能量存储设备的方法.